


Understanding and illustrating the irreversible self-discharge in rechargeable batteries by the Evans Diagram

Xiangjun Pu^{1,2,3} | Yingping Zheng² | Aiping Qi⁴ | Linlong Lyu² |
Guanqiang Ruan⁵ | Yuliang Cao³ | Zhongxue Chen¹  | Zheng-Long Xu²

¹Key Laboratory of Hydraulic Machinery Transients, Ministry of Education, School of Power and Mechanical Engineering, Wuhan University, Wuhan, China

²Department of Industrial and Systems Engineering, The Hong Kong Polytechnic University, Hung Hom, Hong Kong SAR, China

³Hubei Key Laboratory of Electrochemical Power Sources, College of Chemistry and Molecular Sciences, Wuhan University, Wuhan, China

⁴Section of Middle Education, Awu Nine-Year Integrated School in Tanchang, Longnan, China

⁵School of Mechanical Engineering, Automotive Structure and Energy Storage Engineering Center, Shanghai Dianji University, Shanghai, China

Correspondence

Zhongxue Chen, Key Laboratory of Hydraulic Machinery Transients, Ministry of Education, School of Power and Mechanical Engineering, Wuhan University, Wuhan 430072, China.
Email: zxchen_pmc@whu.edu.cn

Zheng-Long Xu, Department of Industrial and Systems Engineering, The Hong Kong Polytechnic University, Hung Hom, Hong Kong SAR, China.
Email: zhenglong.xu@polyu.edu.hk

Funding information

Joint Postdoc Scheme with Non-local Institute from PolyU,
Grant/Award Number: 1-YY4L; National Natural Science Foundation of China, Grant/Award Number: U22A20438; Key R&D Plan of Hubei Province, Grant/Award Number: 2023BAB036; Innovation and Technology Fund (ITF) from the Innovation and Technology Commission, Hong Kong SAR, Grant/Award Number: ITS/126/21

Abstract

As an intermediary between chemical and electric energy, rechargeable batteries with high conversion efficiency are indispensable to empower electric vehicles and stationary energy storage systems. Self-discharge with adverse effects on energy output and lifespan is a long-existing challenge and intensive endeavors have been devoted to alleviating it. Previous reports mainly focused on examining key factors influencing the rate of self-discharge, however, its origination has rarely been revealed from the viewpoint of fundamental electrochemistry. The Evans Diagram, which is a corrosion polarization diagram based on kinetics (corrosion current density) and thermodynamics (potential), is an informative method for analyzing the corrosion process of metals. In this perspective, after an introduction to electrochemical fundamentals, as well as the identical origination of battery self-discharging and metal corrosion, we first transferred the concept of the Evans Diagram to illustrate the origination and evolution of self-discharge in rechargeable batteries. The corresponding Evans Diagram has been proposed for different key factors, which were eventually used as guidance to exploit thermodynamical and kinetical solutions to alleviate the parasitic reactions induced by self-discharge. This contribution is believed to provide new insights towards understanding and regulating self-discharge problems, and promote the establishment of feasible protocols for battery storage in practice.

KEYWORDS

electrochemical viewpoint, Evans Diagram, rechargeable batteries, self-discharge

This is an open access article under the terms of the [Creative Commons Attribution](https://creativecommons.org/licenses/by/4.0/) License, which permits use, distribution and reproduction in any medium, provided the original work is properly cited.

© 2024 The Authors. *Carbon Neutralization* published by Wenzhou University and John Wiley & Sons Australia, Ltd.

1 | INTRODUCTION

Rechargeable batteries with high conversion efficiency are used as a reliable power source for portable electronic devices, electric vehicles and grid-scale energy storage systems.^[1–6] Advanced commercial batteries should hold robust energy/power densities, prolonged lifespan, and durable capacity retention whether in application or storage.^[7–13] Unfortunately, the inevitable parasitic reactions in rechargeable batteries always frustrate the real battery performance away from their initial designs due to irreversible self-discharge,^[14,15] which refers to the progress where a fully or partially charged battery gradually loses its initial stored capacity as self-discharge (Figure 1a,b).^[16] The reasons why self-discharging occurs are associated with the different reversible and irreversible situations. The reversible self-discharge can be attributed to the formation of electron-ion-electrolyte complexes. For example, charge carriers like Li^+ stored in graphite galleries can slowly diffuse to the electrode/electrolyte interface to interact with negatively charged PF_6^- anions, which sacrifices the capacity and lowers the operation voltage. By recharging, the metastable electron-ion-electrolyte groups would dissociate and restore the capacity and voltage loss.^[16] However, the undesirable and spontaneous side reactions between the interface of cathode/electrolyte and anode/electrolyte, as well as corrosion of electrode materials cause irreversible self-discharge even without any connection between the electrodes or any external circuit, and the lost capacity during such process cannot be compensated during recharge. Specifically, the degree of self-discharge depends on the electrode chemistry, electrolyte formulation, the discharge/charge stages, and the storage temperature. Table 1 summarizes the technical parameters for typical battery systems.

Undoubtedly, irreversible self-discharge is detrimental and undesired at both single cell and pack level. For single cells, it would suppress the energy output due to the capacity loss, and the accumulation of undesired side reactions would result in excessive cation loss and shorten cycle life. For larger battery packs, the self-discharge will result in inconsistent charging states among cells during charge (Figure 1c). The unhealthy cell will reach the end of charge earlier than its healthy counterparts, bringing safety issues like dendrite growth, gas emission, thermal runaway even explosions.^[26,27] Overcharging (Figure 1d) is another severe safety concern for the battery system, which causes inferior energy output and brings additional challenges to the battery management system (BMS). For instance, for lithium ion batteries (LIBs) using LiFePO_4 cathode, the overcharging rates of 105%–120% can immediately induce rapid temperature increase and significant capacity loss and brings an additional challenge for BMS.^[28] Therefore, understanding and developing useful methods (Figure 2a) for self-discharge induced by various factors (Figure 2b) in batteries are essential in resolving safety and capacity degradation concerns.

1.1 | The significance of measuring self-discharge

1.1.1 | Predicting faulty cells for factory inspection

Investigating the self-discharge rate of commercial LIBs indicates momentous significance in the industry. During the manufacturing of LIBs, although the materials and manufacturing process from the same batch are

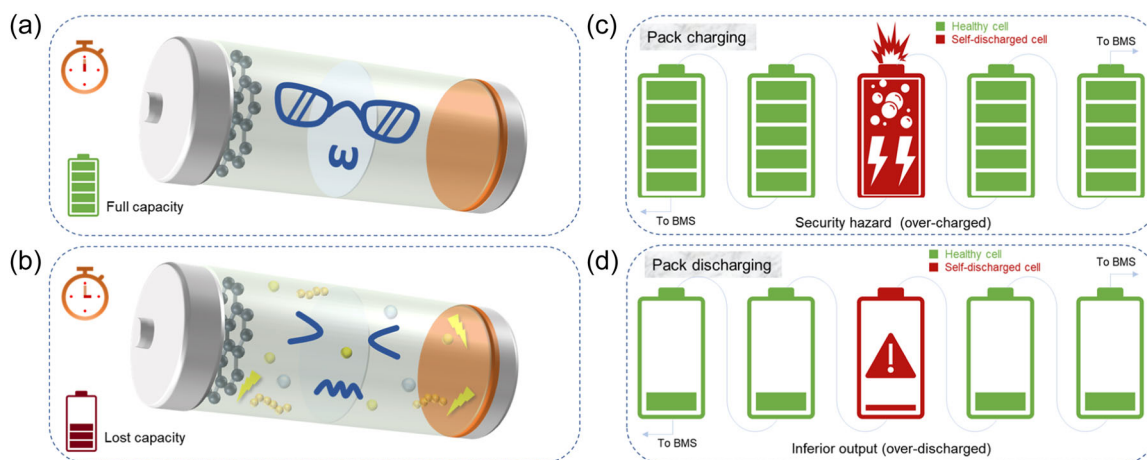


FIGURE 1 Schematic illustration of self-discharge from (a) sufficient to (b) insufficient capacity. The adverse influences to the pack from the self-discharged cell: (c) over-charge to release undesirable heat and gas, and (d) over-discharge leading to inferior energy supply.

TABLE 1 Comparison of technical characteristics among typical battery chemistry.^[17]

Cell chemistry	Power rating	Discharge time	Self-discharge rate	SSD	Possible self-discharge origination
Lead-acid	0–20 MW	Seconds–hours	4%–6%/month	Minutes–days	$\text{PbO}_2 + 2\text{H}_3\text{O}^+ + \text{SO}_4^{2-} \rightarrow \text{PbSO}_4 + 3\text{H}_2\text{O} + 1/2\text{O}_2 \uparrow$ ^[18] $\text{Pb} + \text{H}_2\text{SO}_4 \rightarrow \text{PbSO}_4 + \text{H}_2 \uparrow$ ^[18]
Na-S	50 KW–8 MW	Seconds–hours	~20%/day	Seconds–hours	$2\text{Na} + x\text{S} \rightarrow \text{Na}_2\text{S}_x$ ($2 \leq x \leq 8$) ^[19,20] & Dissolution and shuttling of S_x^{2-} ^[19,20]
ZEBRA	0–300 KW	Seconds–hours	~15%/day	Seconds–hours	$\text{NaAlCl}_4 + 3\text{Na} \rightarrow 4\text{NaCl} + \text{Al}$ $\text{NiCl}_2 + 2\text{Na} \rightarrow 2\text{NaCl} + \text{Ni}$ ^[21]
Li-ion	0–100 KW	Seconds–24 h	2%–3%/month	Minutes–days	Continuous SEI/CEI growth ^[22] ; Dissolution of active materials, ^[23] Side reactions from impurities ^[22,24]
VFB	30 KW–3 MW	Sec–10 h	<0.1%/day	Hours–months	$\text{V}^{2+} + 2\text{VO}_2^+ + 2\text{H}^+ \rightarrow 2\text{VO}^{2+} + \text{H}_2\text{O}$ ^[25] $\text{VO}_2^+ + 2\text{V}^{2+} + 4\text{H}^+ \rightarrow 3\text{V}^{3+} + 2\text{H}_2\text{O}$ ^[25]

Abbreviations: SSD, suitable storage duration; VFB, vanadium flow batteries; ZEBRA, sodium-nickel chloride batteries.

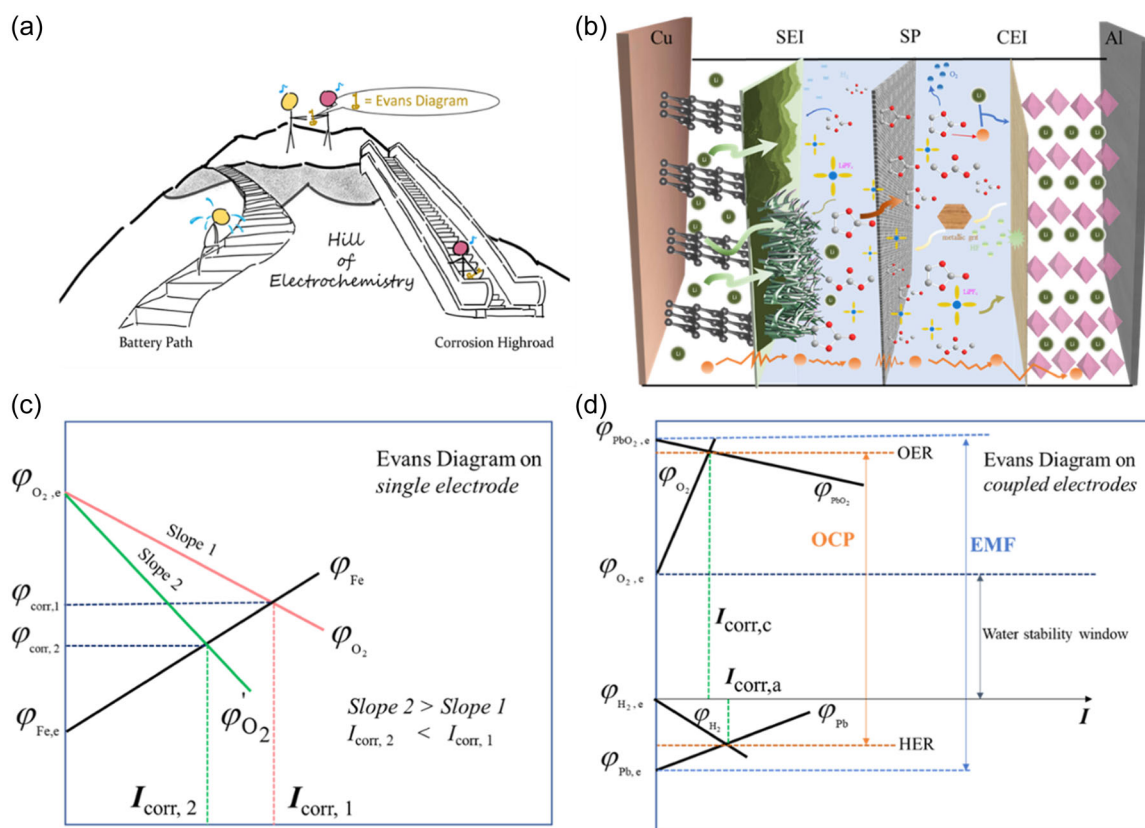


FIGURE 2 (a) The schematic diagram of transferring Evans Diagram from corrosion to battery. (b) The self-discharge issues of lithium ion battery with the configuration of graphite/1M EC-DMC/LiNi_{0.5}Mn_{1.5}O₄ from irreversible electrochemical reaction at various sites (SEI/CEI formation, dendrite growth, active materials dissolution, corrosion of current collector). (c) The concept of the Evans Diagram and its application at a *single electrode* for the corrosion process of iron (different kinetics of oxygen reductive process are presented). (d) The application of the Evans Diagram at *coupled electrodes* with lead-acid battery as an example.

the same, individual battery may have micro-short circuits issues due to the reaction at the cathode/electrolyte, anode/electrolyte, and from impurities in the electrolyte.^[29] In particular, the effect of micro-short

circuits on the battery is unapparent but detrimental. In the short term, the performance of faulty batteries will not be significantly different from that of normal batteries. However, the accumulation of internal

irreversible reactions and micro-short circuits will amplify the unhealthy state of flawed batteries, endangering the safety of battery packs. Therefore, pre-inspection of batteries is necessary to ensure their quality before allowing them to enter the market.

1.1.2 | Matching consistency

Assembling cells into a battery pack needs high consistency of capacity, voltage, internal resistance, and self-discharge rate of individual cells. Once they are assembled into a module with configuration in a series, parallel or a mixture of both, the cell voltage would drop to different levels during shelving due to different self-discharge rates. Upon cycling, the battery performance will gradually degrade and safety concerns like Figure 1c,d will emerge. Therefore, pack matching requires accurate measurement and screening of the self-discharge rate in advance.

1.1.3 | Monitoring the state-of-charge (SoC) and state-of-health (SoH)

The self-discharge rate is vital for SoC and SoH estimation. The correction of measured currents by the self-discharge could improve the estimation accuracy of SoC. The BMS is a key component in managing the smooth operation of the battery pack based on instant detective signals and algorithm, and with the correction of accurate values modified from the self-discharge test, BMS will work under low complexity and increased reliability, thereby guaranteeing the effective optimization of remaining power and prolonging the battery life.

1.2 | The definition and application of Evans Diagram

Evans Diagram, also known as the corrosion polarization diagram, was proposed to interpret the metal corrosion behavior scientifically by Evans in the 19th century, which shows the relationship between current (kinetics) and potential (thermodynamics) for redox reactions. As known to all, corrosion is a spontaneously destructive process for metals exposed to a corrosive environment. For instance, in the presence of air and moisture, corrosion reactions occur on iron by forming products like oxides, hydroxides or sulfides. Fundamentally, as shown in Figure 2c, the equilibrium potential of Fe would increase from $\varphi_{Fe,e}$ to φ_{corr} ; this kind of deviation is called polarization because of electrons over-accumulation and the sluggish diffusion of Fe

containing side-products. Whereas the continuous supply of oxygen consuming the electrons will reduce the polarization, and this is the reason why oxygen is called the depolarizer of iron corrosion. The kinetics difference for the same reaction but a different process could be easily depicted by the slope of the Evans Diagram. For instance, the process by routine 1 (possibly by continuous supply of oxygen or certain catalytic impurities with lower oxygen reduction overpotential) has lower slope value than routine 2, resulting in severe corrosion in routine 1. Conventionally, to capture the complete corrosion-polarization curve, two sets of parameters including corrosion current (i_{corr}) and corresponding corrosion voltage (φ_{corr}) should be obtained for various voltage steps. However, the Evans Diagram as an approximation to the real case could be fulfilled for the same given system only by depicting the relationship from two groups of i_{corr} and φ_{corr} . In which intercept voltage is the metric of thermodynamics, while the current density is related to kinetics. The rationality of applying the Evans Diagram to self-discharge batteries is adequate. In essence, as summarized in Table 2, both corrosion of metals and self-discharge of batteries are irreversible electrochemical reactions on a certain interface.

Therefore, the theory and methodology of Evans Diagram can be feasibly transplanted into self-discharge in rechargeable batteries. Besides at single electrode, as illustrated in Figure 2d where the lead-acid battery was taken as an example, we could further disclose the electrode features on double electrodes. Electromotive force (EMF) is the range between the equilibrium potentials of PbO_2/Pb^{2+} and $PbSO_4/Pb$. Since EMF is larger than water's stability window, at least two pairs of coupled reactions are possible to occur, on the cathode side of the oxygen evolution reaction (OER) and the anode side of the hydrogen evolution reaction (HER), even overpotential is considered. The two side reactions will exhaust the system energy and render a gradual drop of EMF to open circuit voltage (OCP), which is also called terminal voltage. That is, the distinction between

TABLE 2 Identical kinetics and thermodynamics between corrosion of metals and self-discharge of batteries.

Items	Corrosion of metals	Self-discharge of batteries ^a
Spontaneous	✓	✓
Requesting depolarizer	✓	✓
Electrochemical reaction	✓	✓
Reaction at interface	✓	✓
Irreversibility	✓	✓
Depolarization	✓	✓

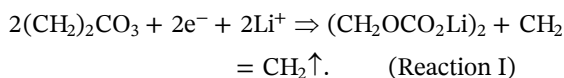
^aOnly the irreversible type of self-discharge is considered.

OCP and EMF is the result of irreversible electrochemical reactions at the electrode/electrolyte interface.

2 | BRIEF ON ELECTROCHEMICAL FUNDAMENTALS

2.1 | Thermodynamics of self-discharge

It is well-known that rust will form when iron is placed in the air. The root cause is a corrosion micro-battery formed between the oxygen and the iron. From the viewpoint of thermodynamics, self-discharge is also a spontaneous reaction with negative Gibbs free energy, incurred by certain impurities (depolarization agents) satisfying the $\Delta G < 0$ condition toward electrodes, similar to that of oxygen as the depolarizer to iron. For instance, ethylene carbonate is the cornerstone to form SEI in commercial LIBs, the driving force of Reaction I, $\Delta_r G$ is below zero due to $\varphi_{\text{EC}/[\text{ECR}], \text{equilibrium}} > \varphi_{\text{Li}^+/\text{Li}, \text{equilibrium}}$:



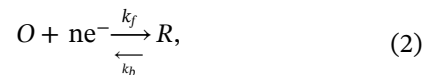
The relationship between Gibbs free energy of $\Delta_r G$ and potentials is given by:

$$\Delta_r G = nFE_r. \quad (1)$$

We have to point out that E_r in Equation (1) is not the electromotive force (EMF) of a designed battery but the driving force of the so-called micro-corrosive battery at anode side following $E_r = \varphi_{\text{EC}/[\text{ECR}], \text{equilibrium}} - \varphi_{\text{Li}^+/\text{Li}, \text{equilibrium}}$. Accordingly, for self-discharge originating from cathode side, there will be another micro-corrosive battery. For instance, in Figure 2d E_r can be decided by $E_r = \varphi_{\text{PbO}_2/\text{Pb}^{2+}, \text{equilibrium}} - \varphi_{\text{O}_2/\text{H}_2\text{O}, \text{equilibrium}}$ at cathode side. During the charge process (SoC become larger gradually), $\varphi_{\text{cathode}, \text{equilibrium}}$ will rise while $\varphi_{\text{anode}, \text{equilibrium}}$ will drop. As a result, the corrosive driving force (E_r) at both sides will be enlarged, leading to much more severe self-discharge, thus the elimination of reactants or reducing the state of charge will be the thermodynamic solution to suppress self-discharge, which will be discussed in details below.

2.2 | Kinetics of self-discharge

If we designate O and R as oxidative and reductive substances, respectively, then the redox reaction can be expressed by the general formula:



where k_f and k_b are the respective forward and backward rate constants. So the corresponding reaction rates (v_f and v_b) are:

$$v_f = k_f C_O(0, t) = \frac{i_c}{nF}, \quad (3.1)$$

$$v_b = k_b C_R(0, t) = \frac{i_a}{nF}, \quad (3.2)$$

where $C_O(0, t)$ and $C_R(0, t)$ are the corresponding concentrations of O and R on electrode surfaces at the time of t , i_c and i_a are corresponding cathodic and anodic current densities.

At equilibrium potential, there is no accumulation of mass and charge, therefore,

$$v_{\text{net}} = v_f - v_b = 0, \quad (4.1)$$

$$i = i_c - i_a = 0. \quad (4.2)$$

Equations (3.1) and (3.2) suggest that the reaction rate (v_f and v_b) of a spontaneous reaction are jointly determined by reactants' concentration (C_O and C_R) and rate constant (k_f and k_b). Therefore, lowering either the reactants' concentration or rate constant will alleviate the self-discharge issues. Regarding the rate constant k , it is an experimental fact that $\ln k$ is always linear with $1/T$ as the so-called Arrhenius empirical equation pointed out as early as 1889:

$$k = A \exp\left(-\frac{\omega}{RT}\right), \quad (5)$$

where ω is the activation energy and A is the pre-exponential factor. Furthermore, it gives a clear recognition that the rate constant is directly reliant on activation energy and temperature. To make narratives more understandable, an illustration based on reaction of $\text{Li}^+ + \text{e}^- \leftrightarrow \text{Li}$ is displayed in Figure 3a: the frequent the ball swings, the greater the possibility (A) for the reaction to happen, and this is the reason why A is also called as frequency factor. Furthermore, ω could be expressed as the change of standard internal energy of activation (ΔU) during the transition state or activated complex. The standard enthalpy of the activation (ΔH) can be decided by:

$$\Delta H = \Delta U + \Delta(PV). \quad (6)$$

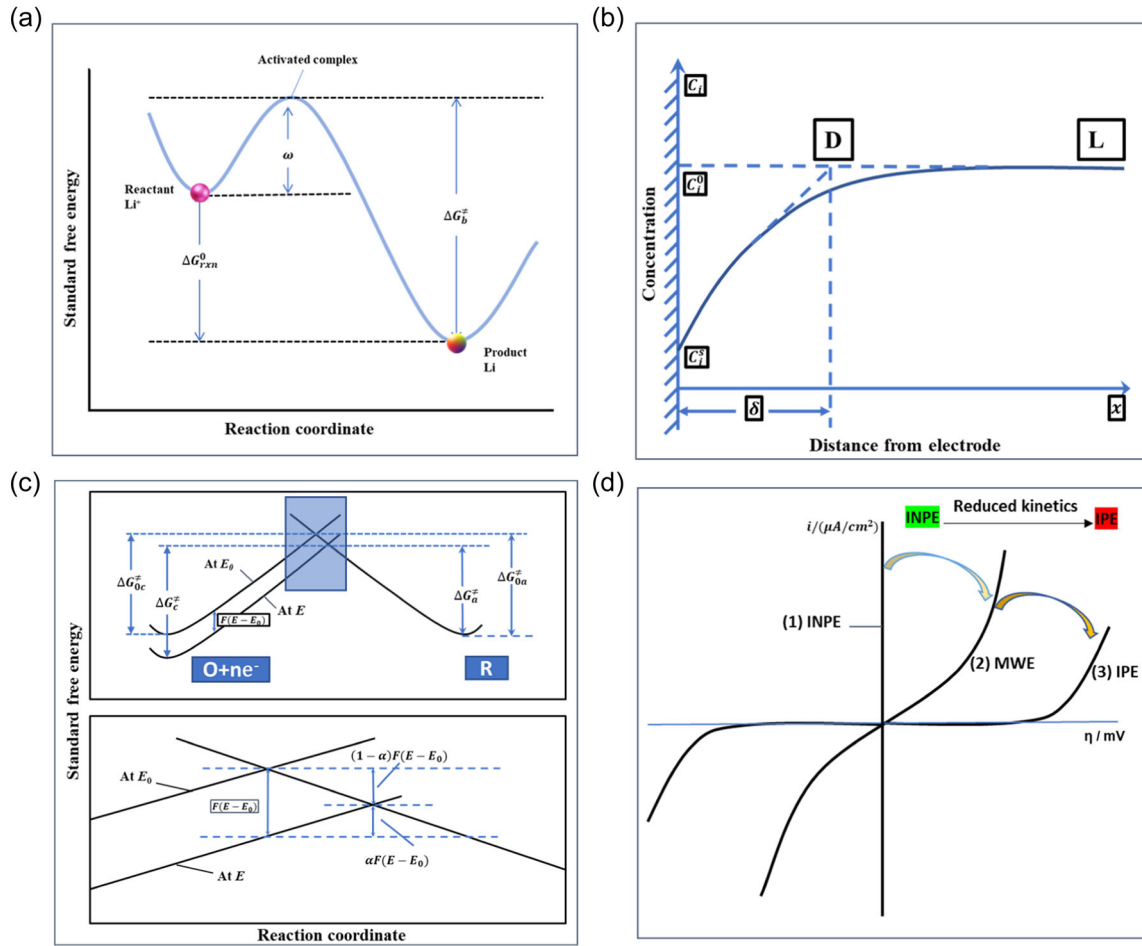


FIGURE 3 (a) Schematic display of activation energy and pre-exponential factor (frequency factor) with $\text{Li}^+ + \text{e}^- \leftrightarrow \text{Li}$ as an example. (b) Reaction rate controlled by mass transfer: the reliance of diffusion current density on the mass concentration near the electrode surface. (c) Effects of potential change on the standard free energies of activation for oxidation (above) and reduction with the enlarged box marked area (below). (d) Reaction rate controlled by activation: overpotential required to deliver net current density in three types of kinds with different exchange current densities (i_o).

The second term could be neglected since the battery is a condensed-phase system. Meanwhile, the internal energy is the sum change of inner microscopic kinetic energy ($\Delta U_{\text{microkin}}$) and the inner microscopic potential energy ($\Delta U_{\text{micropot}}$):

$$\Delta U = \Delta U_{\text{microkin}} + \Delta U_{\text{micropot}}. \quad (7)$$

$\Delta U_{\text{micropot}}$ arises from interaction and in the electrochemical field, it is dependent on the SoC of the electrode. Based on the above analysis, the self-discharge rate is affected by factors including SoC, temperature, activation energy and concentration of reagent. If we could manipulate any factor to create a rate-determining step, then the self-discharge can be decelerated from a kinetic perspective, and there are three types of rate-determining steps in the electrochemistry field related to mass transfer and charge transfer as follows.

2.3 | Reaction controlled by mass transfer

The diffusion polarization is caused essentially by the higher electron mobility than ionic conductivity. As shown in Figure 3b, the diffusion current density (i_d) at steady state can be calculated based on Fick's first law related to surface concentration (C^s), bulk concentration (C^0) and diffusion layer thickness (δ),

$$i_d = nFD \frac{C^0 - C^s}{\delta}. \quad (8)$$

When the surface concentration reaches zero, the limiting diffusion current (i_L) will be determined by the bulk concentration and diffusion layer thickness, as described below:

$$i_L = nFD \frac{C^0}{\delta}. \quad (9)$$

Therefore, if the self-discharge results from impurities, the reasonable way is to remove or reduce their content to lower the i_d value. With mathematical transformation, we have

$$C^s = C^0 \left(1 - \frac{i_d}{i_L} \right). \quad (10)$$

Thereby, the overpotential induced by diffusion can be expressed by,

$$\eta_{\text{diff}} = \frac{RT}{nF} \ln \left(1 - \frac{i_d}{i_L} \right). \quad (11)$$

Equation (11) reminds us that the diffusion overpotential will become much smaller when the concentration or the limiting diffusion current decreases. In other words, the polarization curve will easily enter the diffusion-controlled area in the Evans Diagram when reactants decrease.

2.4 | Reaction controlled by charge transfer

The voltage on an electrode by charge or discharge will influence the Gibbs free energy as well as the activation energy, and eventually the rate constant. The quantitative relation among them is shown in Figure 3c, the rise of potential from E_0 to E will lower the anodic activation energy (decrease of ω_a), while rendering cathodic reaction more difficult to happen (increase of ω_c):

$$\omega'_a = \omega_a - (1 - \alpha)nF(E - E_0), \quad (12.1)$$

$$\omega'_c = \omega_c + \alpha nF(E - E_0), \quad (12.2)$$

where α is the transfer coefficient, n is electrons transferred per formula and F is the Faraday constant. These two equations describe that when the total microscopic potential energy of the reductive product increases $nF\Delta E$ ($\Delta E = E - E_0$), then $\alpha nF\Delta E$ part will hinder the continuation of the cathodic reaction, while the remaining $(1 - \alpha)nF\Delta E$ portion will promote its conjugated anodic reaction. Herein, the net current of i_a during anodic polarization ($\eta_{a,\text{act}} = \varphi_a - \varphi_{a,e}$) and i_c during cathodic polarization ($\eta_{c,\text{act}} = \varphi_{c,e} - \varphi_c$) on a single electrode can be summarized into the well-known Butler–Volmer Equation:

$$i_a = i_0 \{ \exp[(1 - \alpha)n\eta_{a,\text{act}}] - \exp(-\alpha n\eta_{a,\text{act}}) \}, \quad (13.1)$$

$$i_c = i_0 \{ \exp(\alpha n\eta_{c,\text{act}}) - \exp[-(1 - \alpha)n\eta_{c,\text{act}}] \}, \quad (13.2)$$

where i_0 = exchange current density, $f = F/RT$. The second term in Equation (13.1) (or Equation 13.2) can be neglected when η_a (or η_c) $\geq \frac{118}{n}$ mV at 25°C. In this case, the Butler–Volmer Equation will be simplified into the famous Tafel Equation, which means there is only one reaction processing, either forward or backward in Equation (2) when potential shifts tremendously.

If the reaction rate is controlled by the charge transfer process due to activation energy, the overpotential required to deliver net current density will vary. Such kinetic differences are illustrated in Figure 3d, where three types of electrodes with different exchange current densities (i_0) are included. For the ideal nonpolarizable electrode (INPE) with the best kinetics as well as maximum exchange current density, the polarization curve (curve 1) overlaps with the current axis as the potential does not change from its equilibrium state. Although nonpolarizable is a hypothetical definition, some representative electrodes such as Pt|Hg(l)|Hg₂Cl₂(s)|KCl, Ag(s)|AgCl(s)|KCl can be regarded as this type at a certain extent, which is also the fundamental reason why we use them as a benchmark of reference electrodes in the electrochemical field. Another extreme situation is the ideal polarizable electrode (IPE) with minimum i_0 of curve 3, this concept was first introduced in the year 1934.^[30] IPE is also a hypothetical electrode, the reaction of the electrode itself is infinitely sluggish with zero exchange current density when the potential shifted. The typical application of IPE is polarography, where dropping mercury electrode is used as working electrodes with constantly renewable surfaces to measure unknown metal elements. It's a useful electrochemical analysis method with the lowest detection limit of 10⁻⁵ mol L⁻¹. However, in general, most working electrodes (MWE) behave like curve 2 with medium exchange current density when polarization occurs. If the reaction is accelerated, curve 2 will change toward curve 1. Otherwise, curve 2 will change to curve 3 when kinetics decelerated, which could be reached by in-situ or ex-situ at SEI/CEI.

2.5 | Reaction jointly controlled by diffusion and activation

Although reaction rates controlled by mass transfer and charge transfer were discussed separately in the above parts, in fact, electrochemical polarization and diffusion

polarization always coexist for most electrodes at moderate current density: the reaction rate is both influenced by diffusion and charge transfer. Electrochemical polarization determines the reaction rate at low current density, while at high current density diffusion polarization becomes dominating. Under these circumstances, the overpotential for the large cathodic polarization (η_c) as well as large anodic polarization (η_a) can be expressed by,

$$\eta_c = \frac{RT}{\alpha nF} \ln \frac{i_c}{i_0} + \frac{RT}{\alpha nF} \ln \frac{i_L}{i_L - i_c} = \eta_{c,act} + \eta_{c,diff}, \quad (14.1)$$

$$\eta_a = \frac{RT}{(1-\alpha)nF} \ln \frac{i_a}{i_0} + \frac{RT}{(1-\alpha)nF} \ln \frac{i_L}{i_L - i_a} \quad (14.2)$$

$$= \eta_{a,act} + \eta_{a,diff}.$$

The overpotential can be divided into two parts, for instance for the large cathodic polarization, the total overpotential is the sum of electrochemical polarization ($\eta_{c,act}$) in Equation (13.2) and diffusion polarization (η_{diff}) in Equation (11). Therefore, any measure suppressing either the mass transfer process or charge transfer or both of them could lower the self-discharge rate kinetically, which will be discussed in the next section.

3 | EVOLUTION AND ALLEVIATION OF SELF-DISCHARGE

Based on the principles of the Evans Diagram and electrochemical fundamentals above, it's reasonable to illustrate the evolution between kinetic and thermodynamics through the Evans Diagram and propose counter measures to alleviate self-discharge issues induced by side reactions.

3.1 | Controlling the state of charge (thermodynamic solution)

At the given temperature and storage time, cells at high SoC have a greater tendency to reach the end of life than those at low SoC. The reason behind this can be understood in Figure 4a from the perspective of the Evans Diagram that the potential-axis represents thermodynamics. Thereby a huge potential disequilibrium will occur when cells are charged from low SoC to high SoC. According to Equations (12.1) and (12.2), when the over-potential for anodic reaction changes from $\eta_{La,act}$ to $\eta_{Ha,act}$, then the self-discharge at cathode side only needs to overcome reduced activation energy, thus the

corrosion will become severe. This is also applicable to self-discharge at the anode side. Assuming the kinetics remain unchanged with constant slope values, the self-discharge current will increase from $I_{LS,c}$ to $I_{HS,c}$ (the uppercase *S* stands for SoC while the lowercase *c* represents cathodic reaction) at the cathode side, as well as $I_{LS,a}$ to $I_{HS,a}$ at anode side. It was reported in commercial LIBs that higher SoC causes severe degradation dominated by electrolyte decomposition and the loss of active material at the solid electrolyte interface.^[31] Figure 4b shows the normalized capacity and resistance aging time with different SoCs at 50°C. Aggravated capacity degradation and impedance increasement were observed as increasing the SoC degrees,^[32] which is consistent with our theoretical estimations. To conclude, rechargeable batteries should be kept at a low SoC to avoid severe irreversible reactions and thick SEI layers growth from self-discharge.

3.2 | Management of storage temperature

As stated in Equations (3.1) and (3.2), the reaction rate of a spontaneous reaction is determined by both reaction concentration and rate constant. For the given commercial battery systems, the impurities concentrations are the same, then the temperature and activation energy will dominantly affect the reaction rate. From the perspective of the Evans Diagram shown in Figure 5a, at a given charge state (or thermodynamic state) indicated by the same intercept values, the currents will increase from $I_{LT,c}$ to $I_{HT,c}$ (the uppercase *T* stands for temperature while the lowercase *c* represents cathodic reaction) at the cathode side, as well as $I_{LT,a}$ to $I_{HT,a}$ at the anode side. Both changes are clear implications of enhanced kinetics due to the decrease in the absolute value of slopes. Indeed, the remaining total reversible capacity in Figure 5b and the terminal voltage in Figure 5c went through much severe deterioration with the increasing storage temperature. Many literatures argue Arrhenius' law is a feasible semi-empirical approach to quantitatively describe the relationship between degradation and temperature, especially for calendar aging.^[34] However, we still need to keep in mind that Arrhenius law can only be applied to parasitic electrochemical reactions upon aging storage.^[32]

High temperature also increases the activity of the electrolyte and/or impurities since the enhanced rate is constant. Meanwhile, there are other reasons why high temperature aggravates self-discharge. (1) Electrons become more active and easier to penetrate the SEI layer and participate in side-reactions at the interface of the

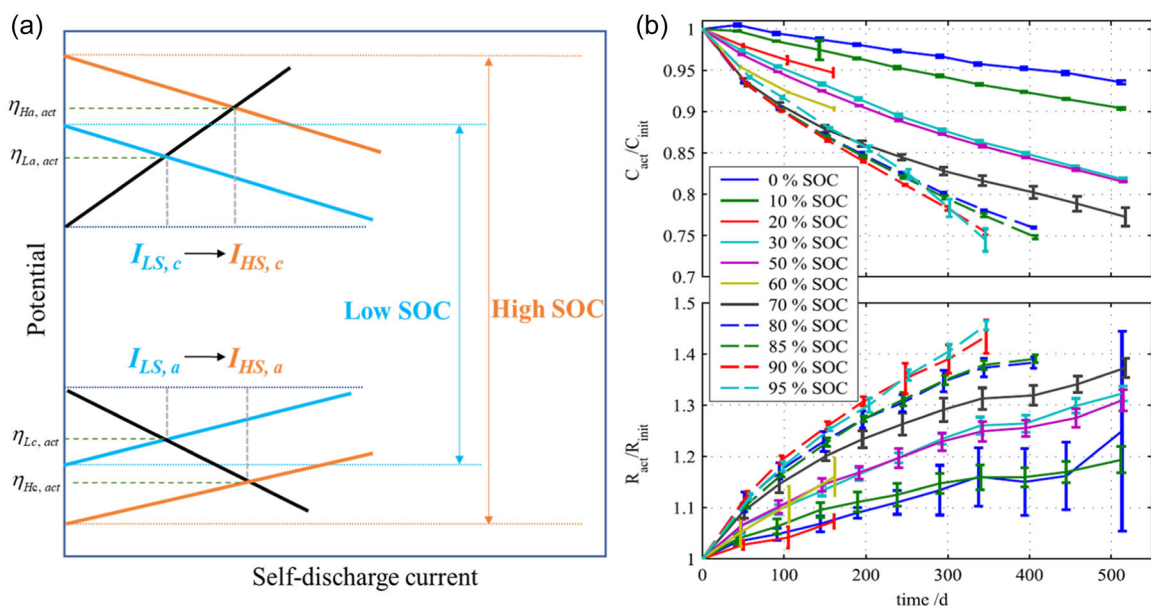


FIGURE 4 (a) The self-discharge rates affected by SoC illustrated by the Evans Diagram. (b) Normalized capacity and resistance over time for calendar aging tests at 50°C. Reproduced with permission: Copyright 2014, Elsevier.^[33]

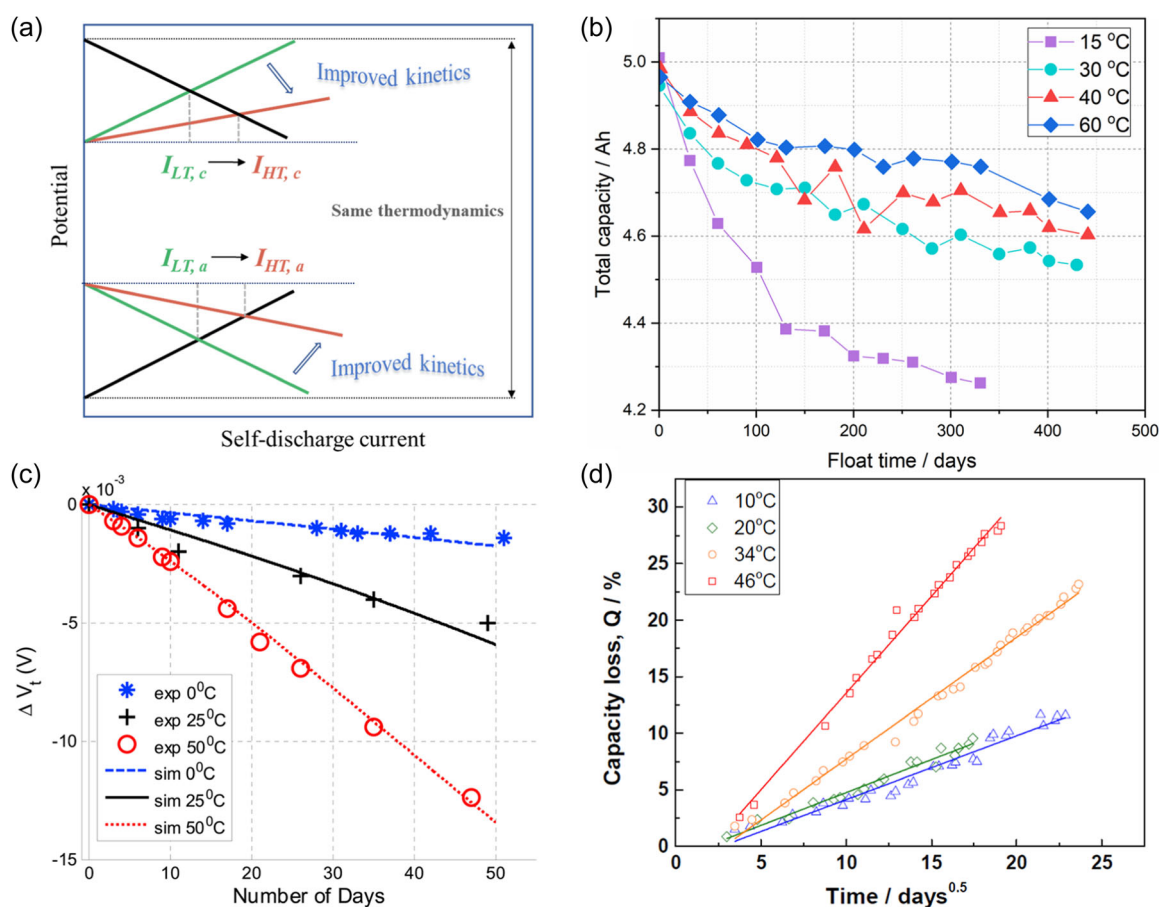


FIGURE 5 (a) The self-discharge rates influenced by temperature elucidated by the means of Evans Diagram. (b) Rebuilt total capacity evolution of LiCoO₂ battery measured monthly at different storage temperature.^[29] (c) Decrease in terminal voltages under self-discharge tests. Reproduced with permission: Copyright 2014, Elsevier.^[35] (d) The percentage of capacity loss is plotted as a function of time^{1/2} relation and corresponding linear fits. The cycle test conditions were at C/2 rate and 10% DOD. Reproduced with permission: Copyright 2014, Elsevier.^[36]

electrolyte/negative electrode at high temperatures. (2) SEI in rechargeable batteries always acts as the passivation layer. However, at high temperatures, it may rupture and dissolve due to instability. After the SEI layer is broken and decomposed, reconstruction of the SEI layer will result in the loss of active materials and electrolytes. At the same time, gases such as H_2 , CO_2 , CO , CH_4 , and C_2H_6 are also generated, deteriorating mechanical properties, and increasing the resistance. (3) High temperature may cause the dissolution of elements with 3d configuration, especially when the cathode material contains manganese, which also leads to performance degradation and capacity loss.

Another factor affecting self-discharge is the storage time (t) because capacity loss (Q_{loss}) is an accumulation of self-discharge current over time,

$$Q_{loss} = \int_0^t i_{self-discharge} \cdot dt. \quad (15)$$

Self-discharge current is nonlinear to the storage time since the growth of the interfacial layer and exhaustion of reactants. In this field, many researchers propose a universal formulation to describe Equation (15) by blending temperature, SoC, as well as exponent-sign (γ) modified storage time together^[36,37]:

$$Q_{loss} = \alpha \cdot \exp(-\beta_1 \cdot T^{-1}) \cdot \exp(-\beta_2 \cdot SOC) \cdot t^\gamma, \quad (16)$$

Where α , β_1 , β_2 are constants, and γ ranges from 0.5 to 1.0 depending on certain systems. For instance, shown in Figure 5d, Verbrugge^[36] predicted the degradation of graphite//LiMn_{1/3}Ni_{1/3}Co_{1/3} + LiMn₂O₄ cell upon time and temperature at a given SoC of 10%. Their result suggested a strong reliance on self-discharge capacities to days^{0.5}, and this $t^{1/2}$ relationship indicates the calendar loss is a diffusion-controlled process.^[36,37] As a matter of fact, temperature rise comes from both the outer and inner parts, thereby storing batteries at low temperatures and with elaborate design on heat dissipation, for instance, the BYD Blade Battery, are feasible methods to alleviate self-discharge.

3.3 | Adjusting diffusion overpotential (kinetic solution)

When the charge transfer process is electrochemically favorable, a reasonable method to alleviate the parasitic reactions in self-discharge is to decrease the reactants' concentration or enlarging the diffusion overpotential to impede reactions from happening, which is

unintentional and can be elucidated by Evans Diagram. As depicted in Equation (9), decreasing the concentration of the depolarization agent will significantly lower the limiting diffusion current (i_L), which will suppress the range of the corrosion polarization curve by rendering it change from charge-transfer limit into concentration limit range quickly. As shown in Figure 6a, for the diffusion-controlled cathodic reactions at the anode side, when the concentration of the depolarization agent decreases from C_2 to C_1 , the corrosion or self-discharge current will drop from $I_{HC,c}$ to $I_{LC,c}$ synchronously (the uppercase C stands for concentration while the lowercase c represents cathodic reaction). Similarly, for diffusion-controlled anodic reactions with different concentrations at the cathode side in Figure 6b, the Evans Diagram can be interpreted in the same way.

However, some depolarizers are unable to be removed completely due to the low content. In such a case, a feasible way is to add a sacrificing agent to capture these impurities, and bring diffusion overpotential to suppress the self-discharge. For instance, trace water is unable to be removed completely, and the existence of fluorine is vital to the formation of SEI but excessive content will lead to the loss of active lithium in the electrolyte.^[39] To cope with this problem, a multi-functional sacrificing agent 3-(trimethylsilyl)-2-oxazolidinone (TMS-ON) was introduced. As shown in Figure 6c, TMS-ON could react with H_2O to generate TMS and ON. Additionally, as it has an N-Si moiety, it shows a high affinity toward HF since the Si atom effectively takes up a fluoride anion to form a penta-valent silane intermediate that subsequently produces trimethylsilyl fluoride.^[38] Consequently, the Evans Diagram for the side reaction will change from C_2 to C_1 as suggested in Figure 6b, and the self-discharge current will decrease from $I_{HC,a}$ to $I_{LC,a}$ simultaneously.

3.4 | Adjusting activation overpotential (kinetic solution)

The principles of kinetically suppressing side reactions through surface modification can be illustrated in Figure 7a. In the relevant Evans Diagram, the above curves are anodic control at the cathode side while the bottom ones are cathodic control at the anode side: after surface modification, the kinetics of the electrode will be lowered, implied by a much steep slope value and decreased modified corrosion current. Therefore, it's reasonable to highlight that this kind of slope change is different from the Evans Diagram in Figure 5a where mainly the kinetics of reactants are shifted. Note that the cathodic and anodic expressions here are opposite to

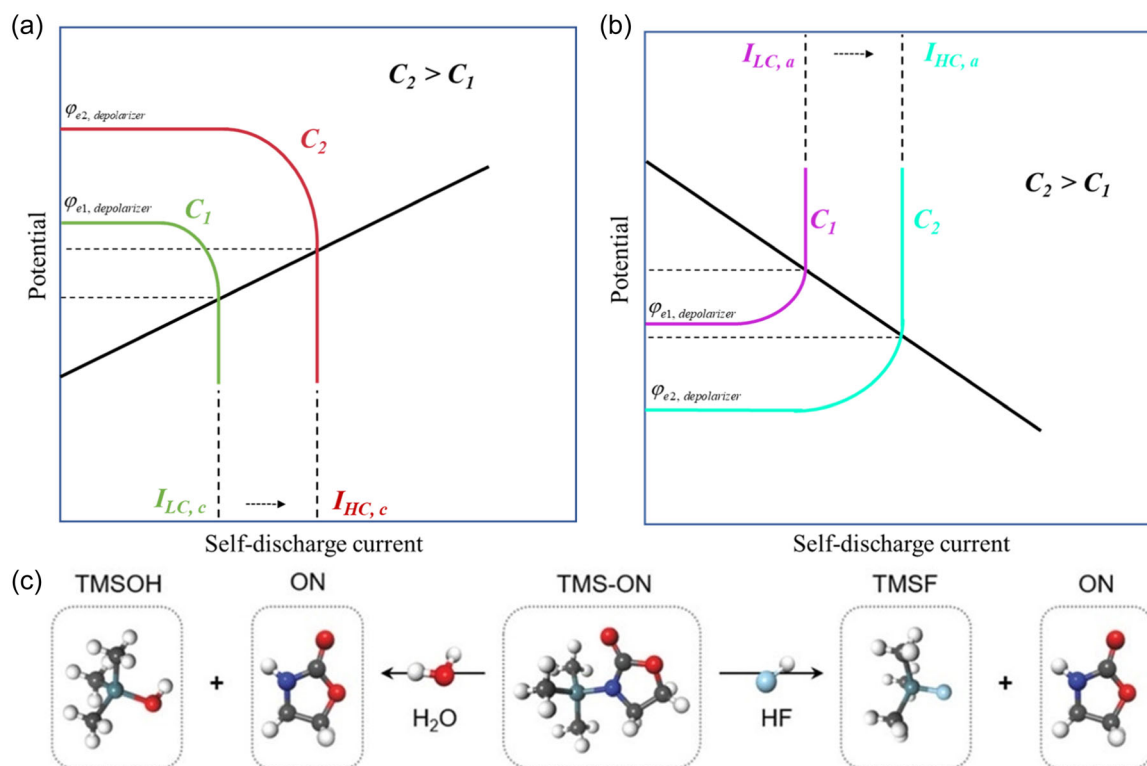


FIGURE 6 Schematic illustration of the reaction inducing self-discharge by the Evans Diagram: (a) cathodic diffusion controlled at anode side and (b) anodic diffusion controlled at the cathode side. (c) HF and H₂O scavenging mechanisms of TMS-ON. Reproduced with permission: Copyright 2020, Wiley.^[38]

those in Figure 6 above, because the modifications are on electrodes instead of on the impurities in the electrolyte as above. To date, many researchers argue there are only two measures ex-situ and in-situ to modify the electrode surface.^[40,41] Regarding the recent reports on interface modification, we propose that there are three ways as follows:

3.4.1 | Ex-situ passivation layer

LiNi_{0.5}Mn_{1.5}O₄ (LNMO) with high average working potential (4.7–4.8 V vs. Li⁺/Li) is an appealing candidate to increase the energy density of Li-ion batteries. However, it suffers from low coulombic efficiency, unignorable self-discharge and poor cyclability in carbonates-based electrolytes mainly due to the increased voltage gap between the equilibrium potential of cathode and carbonate electrolyte. It's confirmed that the oxidation of commercial EC-based electrolytes on LNMO with Tafel-like behavior (temperature and potential activated) is catalyzed on the active material surface (Figure 7b).^[42] Therefore, an effective approach to tackle this interfacial issue is to build an artificial layer. The effects of depositing ultrathin (<1 nm) Al₂O₃ coatings on LNMO

particles using atomic layer deposition (ALD) are presented in Figure 7c. The electrochemical performance of the Al₂O₃ ALD coated LNMO is demonstrated by not only the significantly improved coulombic efficiency, cycle retention, and rate capability, but also the dramatically suppressed self-discharge and dissolution of transition metals.^[43]

3.4.2 | In-situ SEI/CEI

For the LNMO electrode, various borate additives including lithium bis(oxalato)borate (LiBOB), lithium 4-pyridyl trimethyl borate (LPTB), and lithium catechol dimethyl borate (LiCDMB) were used to generate in-situ CEI on its surface (Figure 7d). Though the reaction of the borates on the cathode surface leads to an increase in impedance, the passivation layer on the surface could alleviate the self-discharge issue. The reason behind this is lowered kinetics by in-situ coating, and as shown in Equations (13.1) and (13.2), the change of kinetics can be estimated via the exchange current density (i_0), which could be obtained from Tafel fitting when strong polarization is applied. As unambiguously confirmed by Amine and coworkers, the rule for solvation number of

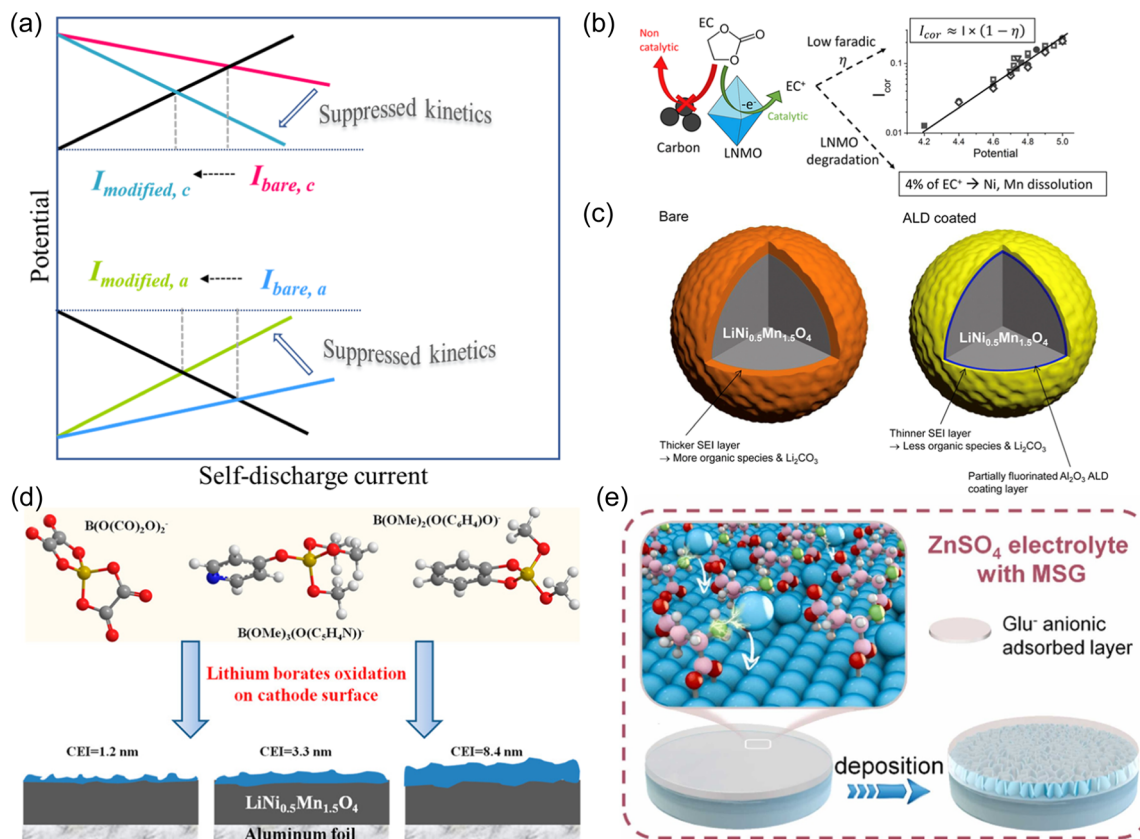


FIGURE 7 The self-discharge rates are influenced by various surface modification methods. (a) The principles of kinetics suppression are interpreted by the Evans Diagram, in which the above is anodic control at the cathode while the bottom is cathodic control at the anode. (b) The oxidation of commercial EC-based electrolyte on LNMO with Tafel-like behavior. Note catalysis on the active material surface rather than the carbon. Reproduced with permission: Copyright 2020, Elsevier.^[42] (c) Ex-situ layer: Al₂O₃ ALD coated LNMO electrodes to alleviate the EC aroused self-discharge. Reproduced with permission: Copyright 2014, Elsevier.^[43] (d) In-situ: CEI generated from various borate additives on LNMO. Reproduced with permission: Copyright 2017, American Chemical Society.^[44] (e) Pseudo film: schematic of Zn/electrolyte interface behaviors during Zn deposition in ZnSO₄ and ZnSO₄ electrolyte with MSG. Reproduced with permission: Copyright 2020, Elsevier.^[45]

fluoroethylene carbonate ≥ 1 will ensure the formation of a stable SEI, and Tafel fitting results showed a decline of exchange current density when the rule is reached, indicating the suppressed kinetics.^[46]

3.4.3 | Pseudo film

Besides the two steadily existing passivation layers to suppress kinetics of self-discharge, another feasible approach is to introduce certain pseudo-protective films by cations or anions adsorption. Yang and colleagues proposed ammonium acetate (NH₄OAc) as a self-regulated Zn/electrolyte interface additive. Before being adsorbed on the Zn surface, the NH₄⁺ induces a dynamic electrostatic shielding layer around the abrupt Zn protuberance to make the Zn deposition uniform, and the OAc⁻ acts as an interfacial pH buffer to suppress the proton-induced side reactions and the precipitation of

insoluble by-products.^[47] Similarly, a monosodium glutamate electrolyte additive is introduced to reconstruct the Zn anode/electrolyte interface and suppress Zn dendrite growth as well as H₂ evolution (Figure 7e). The glutamate anions are preferentially adsorbed on the active sites for Zn corrosion and H₂ evolution, thereby these side reactions inducing self-discharge are largely suppressed.^[45]

4 | CONCLUSION AND OUTLOOK

For the first time, the self-discharge of rechargeable batteries induced by parasitic reactions is elucidated from the sight of the Evans Diagram, which is an effective method used in corrosion science for analyzing the coupled relationship between kinetics and thermodynamics. From the perspective of electrochemistry, self-discharge is a spontaneous reaction involved by both mass transfer and

charge transfer, thus inhibition or restriction of any step will alleviate its deteriorating impact. Accordingly, four factors and their corresponding Evans Diagrams were first outlined point-by-point, followed by proposing four solutions, including low state of charge, low storage temperature, large diffusion overpotential and large activation overpotential to provide theoretical guidance for decelerating self-discharge issues. Overall, this perspective article provides a novel and effective analysis method to inspect the self-discharge of rechargeable batteries from the sight of coupled thermodynamic and kinetic, providing guidelines for the battery community and industrial manufacturers.

AUTHOR CONTRIBUTIONS

Xiangjun Pu: Investigation; methodology; writing—original draft; writing—review and editing. **Yingping Zheng:** Data analysis and curation; formal analysis. **Aiping Qi:** Investigation; methodology. **Linlong Lyu:** Data analysis and curation. **Guanqiang Ruan:** formal analysis. **Yuliang Cao:** Resources; data analysis and curation. **Zhongxue Chen:** Resources; data analysis and curation; supervision; writing—review and editing. **Zheng-Long Xu:** Conceptualization; funding acquisition; supervision; writing—review and editing.

ACKNOWLEDGMENTS

The work described in this paper was supported by the Innovation and Technology Fund (ITF) from the Innovation and Technology Commission, Hong Kong SAR (Project No. ITS/126/21), National Natural Science Foundation of China (U22A20438) and the Key R&D Plan of Hubei Province (2023BAB036). XJ Pu acknowledges the Joint Postdoc Scheme with Non-local Institute from PolyU under project code 1-YY4L. We also acknowledge the design novelty conceived by Mr. AiPing Qi and Ms. ZiYan Fan as well as their contributions to the Figures.

CONFLICT OF INTEREST STATEMENT

The authors declare no conflict of interest.

DATA AVAILABILITY STATEMENT

Data will be made available on request.

ORCID

Zhongxue Chen  <http://orcid.org/0000-0002-1526-7336>

REFERENCES

- [1] J. M. Tarascon, M. Armand, *Nature* **2001**, *414*, 359.
- [2] L. Q. Mai, B. Hu, W. Chen, Y. Y. Qi, C. S. Lao, R. S. Yang, Y. Dai, Z. L. Wang, *Adv. Mater.* **2007**, *19*, 3712.
- [3] X.-P. Gao, H.-X. Yang, *Energy Environ. Sci.* **2010**, *3*, 174.
- [4] R. Tripathi, T. N. Ramesh, B. L. Ellis, L. F. Nazar, *Angew. Chem. Int. Ed.* **2010**, *49*, 8738.
- [5] H. Wang, S. Chen, C. Fu, Y. Ding, G. Liu, Y. Cao, Z. Chen, *ACS Mater. Lett.* **2021**, *3*, 956.
- [6] A. Zhao, T. Yuan, P. Li, C. Liu, H. Cong, X. Pu, Z. Chen, X. Ai, H. Yang, Y. Cao, *Nano Energy* **2022**, *91*, 106680.
- [7] Y. Xu, L. Jiao, J. Ma, P. Zhang, Y. Tang, L. Liu, Y. Liu, H. Ding, J. Sun, M. Wang, Z. Li, H.-L. Jiang, W. Chen, *Joule* **2023**, *7*, 515.
- [8] Z. Zhu, W. Wang, Y. Yin, Y. Meng, Z. Liu, T. Jiang, Q. Peng, J. Sun, W. Chen, *J. Am. Chem. Soc.* **2021**, *143*, 20302.
- [9] Z. Zhu, T. Jiang, M. Ali, Y. Meng, Y. Jin, Y. Cui, W. Chen, *Chem. Rev.* **2022**, *122*, 16610.
- [10] X. Pu, H. Wang, T. Yuan, S. Cao, S. Liu, L. Xu, H. Yang, X. Ai, Z. Chen, Y. Cao, *Energy Stor. Mater.* **2019**, *22*, 330.
- [11] X. Pu, H. Wang, D. Zhao, H. Yang, X. Ai, S. Cao, Z. Chen, Y. Cao, *Small* **2019**, *15*, 1805427.
- [12] X. Pu, D. Zhao, C. Fu, Z. Chen, S. Cao, C. Wang, Y. Cao, *Angew. Chem. Int. Ed.* **2021**, *133*, 21480.
- [13] X. Pu, C. Rong, S. Tang, H. Wang, S. Cao, Y. Ding, Y. Cao, Z. Chen, *Chem. Commun.* **2019**, *55*, 9043.
- [14] H. A. Andreas, *J. Electrochem. Soc.* **2015**, *162*, A5047.
- [15] V. Knap, D.-I. Stroe, M. Swierczynski, R. Teodorescu, E. Schaltz, *J. Electrochem. Soc.* **2016**, *163*, A911.
- [16] R. Yazami, Y. Reynier, *Electrochim. Acta* **2002**, *47*, 1217.
- [17] H. Chen, T. N. Cong, W. Yang, C. Tan, Y. Li, Y. Ding, *Prog. Nat. Sci.* **2009**, *19*, 291.
- [18] P. Rietschi, R. T. Angstadt, *J. Electrochem. Soc.* **1958**, *105*, 555.
- [19] Y.-X. Wang, J. Yang, W. Lai, S.-L. Chou, Q.-F. Gu, H. K. Liu, D. Zhao, S. X. Dou, *J. Am. Chem. Soc.* **2016**, *138*, 16576.
- [20] Q. Guo, S. Li, X. Liu, H. Lu, X. Chang, H. Zhang, X. Zhu, Q. Xia, C. Yan, H. Xia, *Adv. Sci.* **2020**, *7*, 1903246.
- [21] R. Benato, N. Cosciani, G. Crugnola, S. Dambone Sessa, G. Lodi, C. Parmeggiani, M. Todeschini, *J. Power Sources* **2015**, *293*, 127.
- [22] S. E. Sloop, J. B. Kerr, K. Kinoshita, *J. Power Sources* **2003**, *119-121*, 330.
- [23] T. Deutschen, S. Gasser, M. Schaller, J. Siehr, *J. Energy Stor.* **2018**, *19*, 113.
- [24] W. M. Seong, K.-Y. Park, M. H. Lee, S. Moon, K. Oh, H. Park, S. Lee, K. Kang, *Energy Environ. Sci.* **2018**, *11*, 970.
- [25] J. Sun, D. Shi, H. Zhong, X. Li, H. Zhang, *J. Power Sources* **2015**, *294*, 562.
- [26] P. Pei, J. Chen, Z. Wu, *J. Tsinghua Univ.* **2019**, *59*, 53.
- [27] S. Wang, L. Lu, X. Liu, *J. Power Sources* **2013**, *244*, 101.
- [28] M. Kaliaperumal, M. S. Dharanendrakumar, S. Prasanna, K. V. Abhishek, R. K. Chidambaram, S. Adams, K. Zaghib, M. V. Reddy, *Materials* **2021**, *14*, 5676.
- [29] M. Broussely, S. Herreyre, P. Biensan, P. Kasztejna, K. Nechev, R. J. Staniewicz, *J. Power Sources* **2001**, *97-98*, 13.
- [30] V. S. Bagot'skiĭ, *Fundamentals of Electrochemistry*, John Wiley & Sons, **2006**, pp. 178.
- [31] J. C. Burns, A. Kassam, N. N. Sinha, L. E. Downie, L. Solnickova, B. M. Way, J. R. Dahn, *J. Electrochem. Soc.* **2013**, *160*, A1451.
- [32] K. Jalkanen, J. Karppinen, L. Skogström, T. Laurila, M. Nisula, K. Vuorilehto, *Appl. Energy* **2015**, *154*, 160.
- [33] J. Schmalstieg, S. Käbitz, M. Ecker, D. U. Sauer, *J. Power Sources* **2014**, *257*, 325.
- [34] J. de Hoog, J.-M. Timmermans, D. Ioan-Stroe, M. Swierczynski, J. Jaguemont, S. Goutam, N. Omar, J. Van Mierlo, P. Van Den Bossche, *Appl. Energy* **2017**, *200*, 47.

- [35] R. Fu, S.-Y. Choe, V. Agubra, J. Fergus, *J. Power Sources* **2015**, 278, 506.
- [36] J. Wang, J. Purewal, P. Liu, J. Hicks-Garner, S. Soukazian, E. Sherman, A. Sorenson, L. Vu, H. Tataria, M. W. Verbrugge, *J. Power Sources* **2014**, 269, 937.
- [37] S. Grolleau, A. Delaille, H. Gualous, P. Gyan, R. Revel, J. Bernard, E. Redondo-Iglesias, J. Peter, *J. Power Sources* **2014**, 255, 450.
- [38] K. Kim, D. Hwang, S. Kim, S. O. Park, H. Cha, Y. S. Lee, J. Cho, S. K. Kwak, N. S. Choi, *Adv. Energy Mater.* **2020**, 10, 2000012.
- [39] C. Lin, A. Tang, H. Mu, W. Wang, C. Wang, *J. Chem.* **2015**, 2015, 1.
- [40] K. Xu, *Chem. Rev.* **2014**, 114, 11503.
- [41] E. Peled, S. Menkin, *J. Electrochem. Soc.* **2017**, 164, A1703.
- [42] P. Dumaz, C. Rossignol, A. Mantoux, N. Sargent, R. Bouchet, *J. Power Sources* **2020**, 469, 228337.
- [43] J. W. Kim, D. H. Kim, D. Y. Oh, H. Lee, J. H. Kim, J. H. Lee, Y. S. Jung, *J. Power Sources* **2015**, 274, 1254.
- [44] Y. Dong, B. T. Young, Y. Zhang, T. Yoon, D. R. Heskett, Y. Hu, B. L. Lucht, *ACS Appl. Mater. Interfaces* **2017**, 9, 20467.
- [45] Y. Zhong, Z. Cheng, H. Zhang, J. Li, D. Liu, Y. Liao, J. Meng, Y. Shen, Y. Huang, *Nano Energy* **2022**, 98, 107220.
- [46] C. C. Su, M. He, J. Shi, R. Amine, J. Zhang, K. Amine, *Angew. Chem.* **2020**, 132, 18386.
- [47] D. Han, Z. Wang, H. Lu, H. Li, C. Cui, Z. Zhang, R. Sun, C. Geng, Q. Liang, X. Guo, Y. Mo, X. Zhi, F. Kang, Z. Weng, Q. H. Yang, *Adv. Energy Mater.* **2022**, 12, 2102982.

AUTHOR BIOGRAPHIES

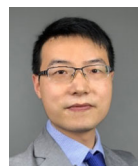


Xiangjun Pu has received the PhD degree in chemistry from Wuhan University (2021). Now he is a postdoc in the group of Prof. Kisuk Kang of Seoul National University. His research interests

focus on fundamental electrochemistry and sustainable materials for rechargeable batteries.



Zhongxue Chen received his BSc degree in (2007) and PhD degree in (2012) from Wuhan University and worked as a visiting scholar at the Pennsylvania State University from 2010 to 2011. Currently, he is an associate professor in the School of Power and Mechanical Engineering at Wuhan University. His research interests focus on energy storage/conversion materials and devices, including battery safety, sodium-ion battery and aqueous batteries.



Zheng-Long Xu is currently an assistant professor in the Department of Industrial and Systems Engineering at The Hong Kong Polytechnic University. He received his BSc in Materials Science and Engineering from Zhejiang University and PhD degree from The Hong Kong University of Science and Technology. His research group at PolyU focuses on the development of new materials and devices for post-Li battery chemistries (i.e., Li-S, Na-ion, and Ca-ion batteries) and operando characterizations (i.e., in situ TEM).

How to cite this article: X. Pu, Y. Zheng, A. Qi, L. Lyu, G. Ruan, Y. Cao, Z. Chen, Z.-L. Xu, *Carbon Neutralization* **2024**;3:94–107.

<https://doi.org/10.1002/cnl2.106>